Dynamics of Block Copolymer Micelles Revealed by X-Ray Intensity Fluctuation Spectroscopy

S. G. J. Mochrie,[1] A. M. Mayes,[1] A. R. Sandy,[1] M. Sutton,[2] S. Brauer,[3]
G. B. Stephenson,[4] D. L. Abernathy,[5] and G. Grübel[5]
[1]*Center for Materials Science and Engineering, Massachusetts Institute of Technology, Cambridge, Massachusetts 02139*
[2]*Department of Physics, McGill University, Montréal, Québec, Canada*
[3]*Advanced Photon Source, Argonne National Laboratory, Argonne, Illinois 60439*
[4]*Materials Science Division, Argonne National Laboratory, Argonne, Illinois 60439*
[5]*European Synchrotron Radiation Facility, 38043 Grenoble, France*
(Received 8 November 1996)

We report x-ray intensity fluctuation spectroscopy measurements of the equilibrium dynamics of polymer micelle liquids, composed of polystyrene-polyisoprene block copolymer micelles within a polystyrene homopolymer matrix. The equilibrium dynamics were investigated for times between one and several hundred seconds, and for wave vectors from 0.003 to 0.015 Å^{-1}, far beyond wave vectors that can be studied with visible light. A wave-vector-dependent diffusion coefficient is found. [S0031-9007(97)02392-2]

PACS numbers: 61.41.+e, 61.10.Yh

Block copolymers show a variety of microstructures as a result of their amphiphilic molecular architectures [1], motivating continuing investigations of their structure, thermodynamics, and rheology. However, it has not generally been possible to study the molecular-scale dynamics of block copolymer melts, because the length scale of the microstructure is several tens of nanometers—determined by the size of the polymers—and is thus inaccessible to light scattering techniques; while the relevant time scales are slower than can be easily studied by neutron scattering [2].

The introduction of high-brilliance synchrotron sources now allows for intensity fluctuation spectroscopy measurements using coherent x rays (XIFS), enabling investigations of molecular-scale dynamics [3–6]. XIFS was recently demonstrated in small-angle scattering studies of the diffusion of dilute gold [5] and palladium [6] colloidal particles, suspended in glycerol. In the present paper, we report an XIFS study of the dynamics of mixtures of polystyrene-polyisoprene block copolymers with polystyrene homopolymer. The mixtures lie in a micellar region of the phase diagram, forming either spherical or wormlike micelles [7–9]. There are correlations among the micelles, which give rise to a peak in the static scattering function at ~0.012 Å^{-1}, corresponding to liquidlike micellar order. The glass transition of the homopolymer matrix occurs at ~360 K. It follows that the micelles are mobile only above ~360 K. We have investigated the dynamics of these polymer micelle liquids for times between one and several hundred seconds, and for wave vectors from 0.003 to 0.015 Å^{-1}, extending far above what can be achieved with visible light and including the peak in the static structure factor.

Copolymer synthesis was performed via anionic polymerization under inert gas, yielding P (S-*b*-I) with a styrene number fraction of $f_s = 0.5$, $\bar{M}_w = 89.1k$, and $\bar{M}_w/\bar{M}_n = 1.02$. ($\bar{M}_w$ and $\bar{M}_n$ are the weight- and number-averaged molecular weights, respectively.) The mixtures were prepared by dissolution in toluene, followed by methanol precipitation. After drying, samples were hot pressed into 1 mm diameter, 0.5 mm thick Al sample holders and vacuum annealed at 150 °C. For the x-ray studies, the samples were held under vacuum, and at constant temperature to within ±0.1 °C. The XIFS experiments were carried out at beam line ID10A (TROIKA) at the European Synchrotron Radiation Facility (ESRF) and employed undulator radiation with an energy of 8.2 keV and a bandwidth of $\Delta\lambda/\lambda = 0.013$ [10]. A mirror deflected these x rays out of the undulator central cone onto the sample. The source, 46 m upstream, was 54 μm in the vertical direction. Horizontal slits, 28 m upstream, were adjusted to 250 μm to set the effective horizontal source size. For XIFS studies several criteria must be met: The beam size should be smaller than the transverse coherence length $(\lambda d/2R)$, where λ is the x-ray wavelength, d is the source size, and R is the distance to the source. A pinhole aperture of diameter $d_p = 7$ μm (85 mm upstream of the sample) met this condition, yielding $\sim 2 \times 10^9$ x rays per second. In addition, the maximum optical path length difference should be less than the longitudinal coherence length $(\lambda^2/\Delta\lambda)$, requiring that $\Delta\lambda/\lambda < \lambda/2W \sin^2\theta$ and $\Delta\lambda/\lambda < \lambda/d_p \sin 2\theta$, where W is the sample thickness and 2θ is the scattering angle. These conditions were satisfied for wave vectors up to ~0.03 Å^{-1}. Scattered x rays were collected using a Princeton Instruments CCD array detector, 1.25 m from the sample. The CCD pixel size was 22×22 μm^2. Each data set was acquired as a series of 1000 1.00 s exposures, separated by 0.24 s for readout. Measurements to determine the static scattering cross section were carried out at beam line X20A at the National Synchrotron Light Source using a point detector.

On initial exposure to the beam at ID10A, the overall scattered intensity was observed to decrease by a factor of ~2 over a period of ~200 s. Subsequently, the intensity remained constant in time. We do not understand this

observation. However, the scattering line shape obtained at ID10A reproduced that found at X20A, where no initial decrease in intensity was observed (see below). All of the ID10A data presented in this paper correspond to times at least 1200 s after initial exposure. It may be noted that the flux in the XIFS measurement ($\sim 4 \times 10^{13}$ s^{-1} mm^{-2}) was $\sim$100 times higher than at X20A, but not substantially higher than in some other synchrotron x-ray studies of similar polymer systems [11].

Figure 1(a) shows the average of 500 CCD exposures obtained at 293 K for a mixture containing 17 wt. % P(S-*b*-I) and $\bar{M}_w = 12.7k$ PS (sample I), which forms spherical micelles. Figure 1(b) shows the scattering from the same sample at 393 K, also averaged over 500 exposures. The images comprise 340 $\times$ 200 CCD pixels, corresponding to a wave vector range from 0.0015 to 0.0143 Å^{-1} in the vertical and from -0.0109 to 0.0109 Å^{-1} in the horizontal. The strong scattering at small wave vectors (shown as pink, violet, and blue), including the vertical streaks, originates at the pinhole and in guard slits before the sample. At larger wave vectors, scattering from the sample appears as green, yellow, and red, depending on the intensity. The grainy appearance of Fig. 1(a) in this region constitutes speckle, as expected for a disordered material under coherent illumination.

The speckle is static at 293 K, corresponding to a frozen arrangement of micelles. By contrast, speckle in the sample scattering is not apparent in Fig. 1(b). We may infer that at 393 K the micelles are mobile and that their thermal motions cause the instantaneous speckle to fluctuate in time, resulting in a smoother time-averaged intensity. To determine the characteristic times of the sample, we computed the autocorrelation for each pixel as a function of delay time (t) [5,12]: $g_2(t) = (n - t)\sum_{s=t+1}^{n} i_s i_{s-t}/m_0 m_1$, where n is the number of time steps, i_s is the intensity at time step s, $m_0 = \sum_{s=1}^{n-t} i_s$, and $m_1 = \sum_{s=t-1}^{n} i_s$. To determine the variation versus wave vector (Q), we averaged $g_2(t)$ over all pixels within successive rings of width $\Delta Q = 0.000\,32$ Å^{-1} (five pixels). The resultant, baseline-subtracted autocorrelation is shown versus time for three representative wave vectors in Fig. 2. We have fit the autocorrelation at each wave vector to an exponential decay: $g_2(t) = A + Be^{-t/2\tau_Q}$, where τ_Q is the characteristic time at wave vector Q. This model, shown as the solid lines in Fig. 2, provides a good description of the data, and we believe that the fitted time constants sensibly characterize the decay of intensity correlations.

In Fig. 3(a) are plotted the fitted values of τ_Q versus Q for 393 and 398 K. The time constants at a given wave vector are different by a factor of $\sim$3 at the two temperatures, but the variation versus wave vector appears similar: The decay times are largest at the smallest wave vectors studied (0.0027 Å^{-1}), and decrease rapidly for wave vectors increasing to 0.007 Å^{-1}. Between 0.007 and 0.012 Å^{-1}, they are approximately constant or increase slightly. Eventually, they decrease again for wave vectors above 0.012 Å^{-1}. This behavior appears more complicated than long-wavelength diffusion, for which $\tau_Q = 1/DQ^2$ [6], where D is a micelle diffusion constant. The discrepancy is highlighted in Fig. 3(b), which plots $k_B T \tau_Q Q^2/\eta = k_B T/D\eta$ versus Q, where η is the homopolymer viscosity. Data at 393 and 398 K collapse to a single curve, suggesting that τ_Q is proportional to η [13].

Evidently, $k_B T/D\eta$ approaches a constant at small wave vectors, but increases to a maximum near 0.012 Å^{-1}. To make sense of this observation, we note that $1/\tau_Q$ is the frequency width of the dynamic structure factor $[S(Q, \omega)]$, which exhibits two pertinent properties [14]: First, the frequency integral of $S(Q, \omega)$ is the static structure factor $S(Q)$. Second, the second moment of $S(Q, \omega)$ obeys the

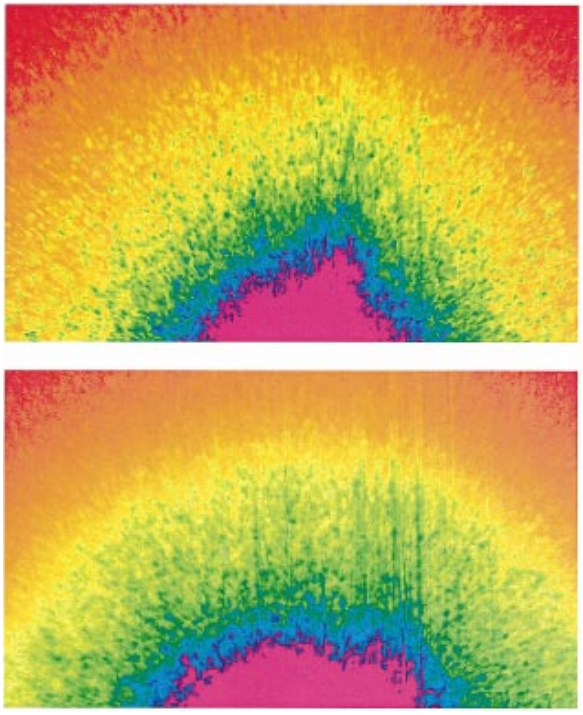

FIG. 1(color). Rainbow-scale CCD image of the scattering from sample I at (a) 293 K and (b) 393 K.

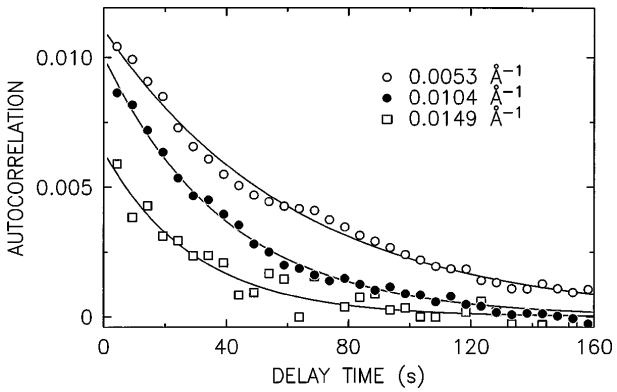

FIG. 2. Autocorrelation vs time for three wave vectors at 393 K. Solid lines correspond to an exponential decay vs time.

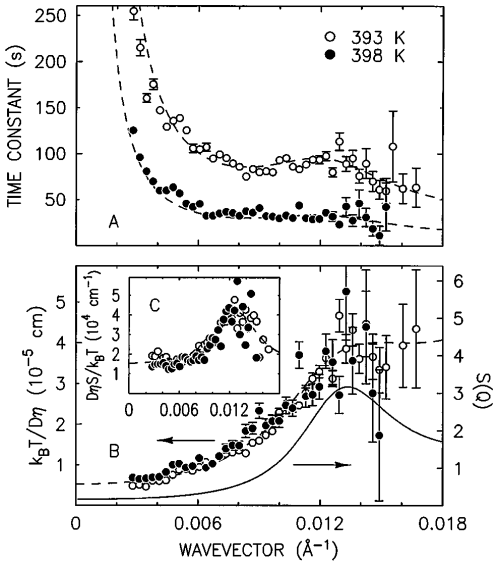

FIG. 3. (a) τ_Q vs Q, (b) $k_BT/D\eta$ vs Q, and (c) $D\eta S(Q)/k_BT$ vs Q for sample I, using $\eta = 2.2 \times 10^5$ and 7.8×10^4 poise at 393 and 398 K, respectively. The solid line in (b) shows $S(Q)$. Dashed lines in (a)–(c) are guides to the eye.

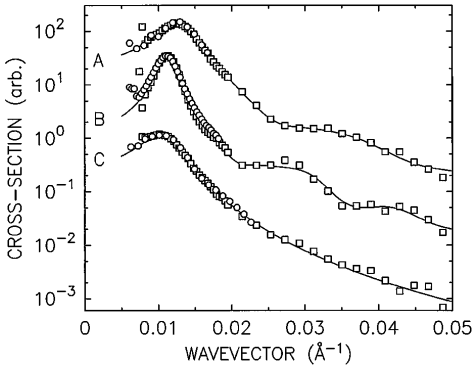

FIG. 4. Scattering cross section vs Q obtained at ID10A (circles) and X20A (squares) for (a) sample I at 398 K, (b) sample II at 398 K, and (c) sample III at 413 K. The solid lines show the models discussed in the text. Each data set is scaled arbitrarily for clarity of display.

sum rule

$$\int_{-\infty}^{\infty} d\omega\, \omega^2 S(Q,\omega) = Q^2 k_B T/M \qquad (1)$$

for all values of Q, where M is a micelle effective mass [14]. In addition, for particles in a viscous medium, $S(Q,\omega)$ at low frequencies takes the form [14]

$$S(Q,\omega) \simeq \frac{S(Q)}{\pi} \frac{DQ^2}{\omega^2 + (DQ^2)^2}\,. \qquad (2)$$

The frequency integral of Eq. (2) is $S(Q)$. However, Eq. (2) does not obey the sum rule. A simple remedy is to suppose that Eq. (2) is valid up to some maximum frequency, ω_c, but that $S(Q,\omega) \simeq 0$ for frequencies greater than ω_c. Then, the sum rule is satisfied, and, moreover, implies that the diffusion coefficient is wave-vector dependent [15], so that $k_BT/D\eta \simeq 2M\omega_c S(Q)/\pi\eta$. In this context, it is remarkable that the data as displayed in Fig. 3(b) are reminiscent of a liquid structure factor. To explore the relationship between $S(Q)$ and D, we have determined $S(Q)$ by fitting the static scattering cross section.

The background-subtracted cross section at 398 K, obtained by circularly averaging CCD images, is shown in Fig. 4(a) as circles. To within a scale factor, these data reproduce results obtained at X20A, shown as squares. For a fluid of spherical micelles, the cross section is well described [9] by

$$d\sigma/d\Omega = r_0^2 N(\rho_{PS} - \rho_{PI})^2 \nu^2 |F(Q)|^2 S(Q)\,, \qquad (3)$$

where r_0 is the Thomson radius, N is the number of micelles, ρ_{PI} and ρ_{PS} are the electronic densities of PS and PI, respectively, $F(Q)$ and ν are the form factor and volume, respectively, of the PI core, and $S(Q)$ is the static structure factor of a hard-sphere fluid. The location and width of the first peak in the cross section at small wave vectors is determined largely by the hard-sphere radius (R) and the hard-sphere volume fraction (ϕ), while the location and depth of the minima at larger wave vectors are determined by the mean radius of the PI cores (a) and the corresponding standard deviation (σ), respectively. The solid line in Fig. 4(a) is the best fit of Eq. (3) to the X20A data. The parameters so obtained are $R = 237$ Å, $\phi = 0.302$, $a = 181$ Å, and $\sigma = 0.181a$, indicating an aggregation number of 305 ± 50 for the micelles in sample I, generally consistent with what may be expected on the basis of Ref. [9].

The solid line in Fig. 3(b) is the hard-sphere-fluid structure factor inferred from R and ϕ. $S(Q)$ generally mimics the variation of $k_BT/D\eta$ versus Q, consistent with the requirements of the sum rule. However, the peak of $S(Q)$ is more pronounced than that of $k_BT/D\eta$. This is quantified in Fig. 3(c), which plots the ratio $D\eta S/k_BT$ versus Q. Evidently, $D\eta S/k_BT$ shows a maximum at a wave vector that is similar to the wave vector of the peak in $S(Q)$. Remarkably, similar behavior is found in light scattering studies of dense systems of large colloidal particles, whose interactions approximate those of hard spheres [16]. In this context, the deviation of $D\eta S/k_BT$ from a constant is ascribed to hydrodynamic interactions between the colloidal particles, mediated by the suspending medium [17].

We present in Fig. 5(a) results for the characteristic times versus wave vector of 29 wt. % P(S-*b*-I) in 3.7k PS (sample II) at 398 K, which also forms spherical micelles. The background-subtracted cross section for this sample is shown in Fig. 4(b), and shows a narrow peak, corresponding to extended correlations between micelles. The best fit of Eq. (3) is the solid line and yields $\phi = 0.446$. $R = 299$ Å, $a = 222$ Å, and $\sigma = 0.146a$. It is striking that the characteristic time [Fig. 5(a)] displays a peak at the same wave vector as the structure factor. However, as is clear from Fig. 5(b), the peak in $S(Q)$ is more pronounced than the peak in $k_BT/D\eta$. The considerably smaller diffusion coefficient of sample II, compared to sample I, may

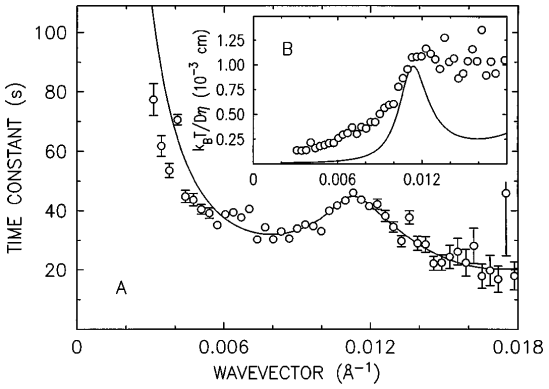

FIG. 5. (a) τ_Q vs Q and (b) $k_BT/D\eta$ vs Q for sample II at 398 K, using $\eta = 3.0 \times 10^3$ poise. The line in (a) is a guide to the eye. The line in (b) is 4×10^{-4} (cm)$S(Q)$.

reflect incipient crystallization of the micelle fluid at larger volume fractions.

Beyond the spherical micelle liquids described so far, it is especially interesting to study materials that self-assemble into more complex morphologies. For example, Fig. 4(c) shows the scattering cross section for 17 wt. % P(S-*b*-I) in 24*k* PS at 413 K (sample III), which forms wormlike micelles [8,18]. Consistent with this, the scattering intensity does not display oscillations at large wave vectors. However, there is a peak of the scattering cross section at 0.01 Å^{-1}, indicating correlations between micelles. In fact, we find that the cross section is well described by $d\sigma/d\Omega = A/(1 - BQ^2 + CQ^4)$, where A, B, and C are constants [solid line in Fig. 4(c)]—a form often used to describe the scattering from microemulsions. Figures 6(a) and 6(b) show the values of τ_Q and $k_BT/D\eta$, respectively, versus Q. In the region of the peak in the scattering, $k_BT/D\eta$ appears to cross over from one value at lower wave vectors to another at higher wave vectors.

In conclusion, we have performed XIFS studies of polymer micelle liquids, composed of spherical and wormlike micelles. For both morphologies, we find a wave-vector-dependent inverse diffusion coefficient, which, in the case of spherical micelles, exhibits a weak peak at the same wave vector as the peak in the static structure factor. Finally, we note that technical improvements can be expected to soon lead to signal rates higher by a factor of $\sim 10^3$, greatly expanding potential applications of XIFS in studies of polymers and soft condensed matter, in general.

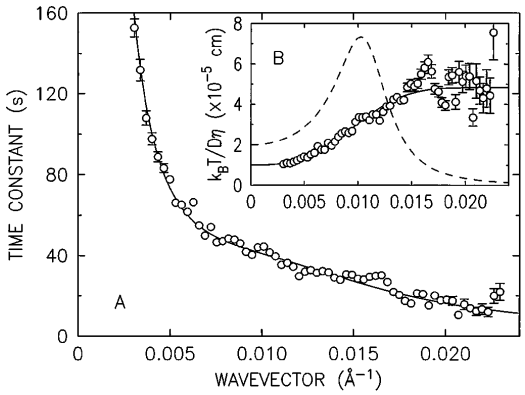

FIG. 6. (a) τ_Q vs Q and (b) $k_BT/D\eta$ vs Q for sample III at 413 K, using $\eta = 7.7 \times 10^4$ poise. The dashed line in (b) shows the scattering line shape. Solid lines in (a) and (b) are guides to the eye.

We would like to thank B. Carvalho, S. Dierker, G. Kellogg, and I. McNulty for valuable discussions, and P. Feder and H. Gleyzolle for technical assistance. We are especially grateful to I. McNulty for participation in the ID10A measurements, and O. Tsui for participation in the X20A measurements. Work at MIT was supported by the NSF (Grants No. DMR-9312543 and No. DMR-9357602), and at ANL by the U.S. DOE under Contract No. W-31-109-ENG-38.

[1] F. S. Bates and G. H. Fredrickson, Annu. Rev. Phys. Chem. **11**, 525 (1990).
[2] D. Richter, B. Farago, L. Fetters, J. Huang, B. Ewen, and C. Lartigue, Phys. Rev. Lett. **64**, 1389 (1990).
[3] M. Sutton, S. G. J. Mochrie, T. Greytak, S. E. Nagler, L. E. Berman, G. A. Held, and G. B. Stephenson, Nature (London) **352**, 608 (1991).
[4] S. Brauer, G. B. Stephenson, M. Sutton, R. Brüning, E. Dufresne, S. G. J. Mochrie, G. Grübel, J. Als-Nielsen, and D. L. Abernathy, Phys. Rev. Lett. **74**, 2010 (1995).
[5] S. Dierker, R. Pindak, R. M. Fleming, I. K. Robinson, and L. E. Berman, Phys. Rev. Lett. **75**, 449 (1995).
[6] T. Thurn-Albrecht, W. Steffen, A. Patkowski, G. Meier, E. W. Fisher, G. Grübel, and D. L. Abernathy (unpublished).
[7] L. Leibler, H. Orland, and J. Wheeler, J. Chem. Phys. **79**, 3550 (1983).
[8] A. Mayes and M. Olvera de la Cruz, Macromolecules **21**, 2543 (1988).
[9] D. J. Kinning, E. L. Thomas, and L. J. Fetters, J. Chem. Phys. **90**, 5806 (1990).
[10] D. L. Abernathy, G. Grübel, S. Mochrie, A. Sandy, G. Stephenson, N. Mulders, M. Sutton, S. Brauer, and I. McNulty (unpublished).
[11] C. Harkless, M. Singh, S. Nagler, G. Stephenson, and J. Jordan-Sweet, Phys. Rev. Lett. **64**, 2285 (1990).
[12] A. Wong and P. Wilzius, Rev. Sci. Instrum. **64**, 2547 (1993).
[13] G. C. Berry and T. G. Fox, Adv. Polym. Sci. **5**, 261 (1967). We have used $\ln\eta = \ln M - 7.4 + 28/[T(K) - 307 + 6 \times 10^4/M]$.
[14] S. W. Lovesey, *Theory of Neutron Scattering from Condensed Matter* (Oxford University Press, Oxford, 1984), Vol. 1, see especially p. 247.
[15] J. Brown, P. Pusey, J. Goodwin, and R. Ottewill, J. Phys. A **8**, 664 (1975).
[16] W. van Megan, R. H. Ottewill, S. M. Owens, and P. N. Pusey, J. Chem. Phys. **82**, 508 (1985).
[17] C. Beenakker and P. Mazur, Physica (Amsterdam) **126A**, 349 (1984).
[18] G. Porte, J. Appell, and Y. Poggi, J. Phys. Chem. **84**, 3105 (1980).